Electronic Supplementary Material (ESI) for Journal of Materials Chemistry A.

Electronic Supplementary Information (ESI)

Influence of Pt Size and CeO_2 Morphology at the Pt-CeO_2 Interface in CO Oxidation

Sinmyung Yoon, ‡[a] *Hyunwoo Ha,*‡[b] *Jihun Kim,*[a] *Eonu Nam,*[a] *Mi Yoo,*[b] *Beomgyun Jeong,*[c] *Hyun You Kim,* *[b] *and Kwangjin An* *[a]

[a]School of Energy and Chemical Engineering, Ulsan National Institute of Science and Technology (UNIST), Ulsan 44919, Republic of Korea

[b]Department of Materials Science and Engineering, Chungnam National University, 99 Daehak-ro, Yuseong-gu, Daejeon 34134, Republic of Korea

[c]Research Center for Materials Analysis, Korea Basic Science Institute (KBSI), Daejeon 34133, Republic of Korea

Corresponding Authors

*E-mail: kimhy@cnu.ac.kr (H.Y.K); kjan@unist.ac.kr (K.A)

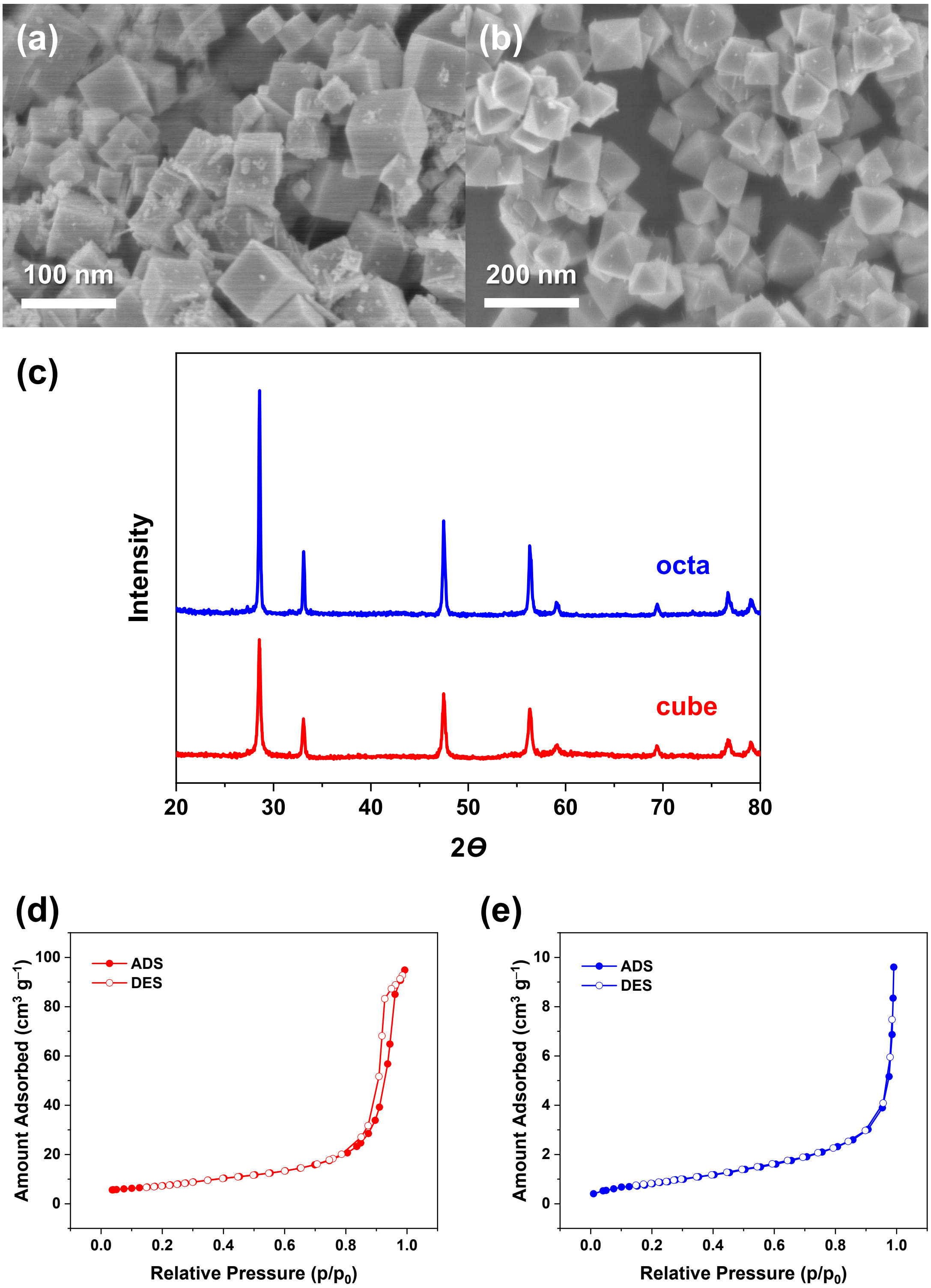

Fig. S1 (a, b) SEM images of (a) CeO_2 cubes and (b) CeO_2 octahedra. (c) XRD patterns of CeO_2 cubes and octahedra. (d, e) N_2 adsorption-desorption isotherms of (d) CeO_2 cubes and (e) CeO_2 octahedra.

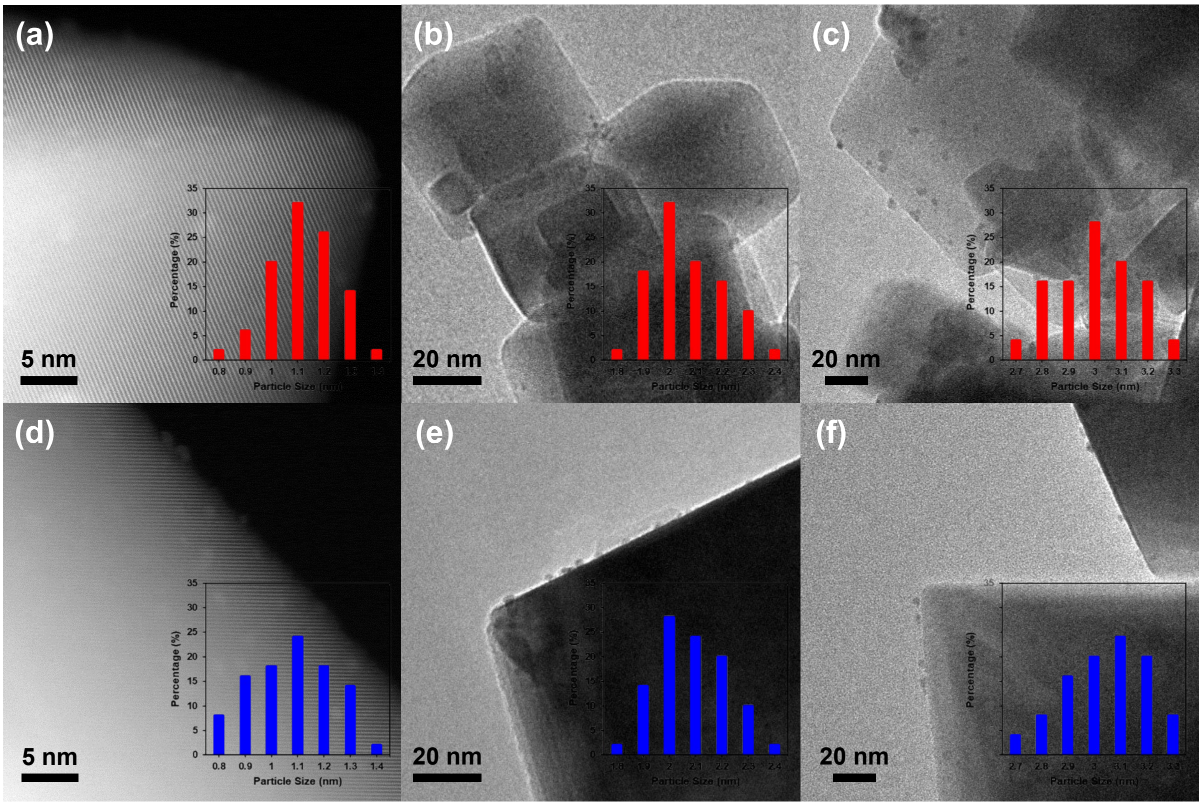

Fig. S2 HAADF-STEM and TEM images, and Pt particle size distribution histograms (inset) of Pt/CeO_2 catalysts: (a) PCC-1, (b) PCC-2, (c) PCC-3, (d) PCO-1, (e) PCO-2, and (f) PCO-3.

Table S1. Pt concentration, average particle size of Pt/CeO_2 catalysts, and CO chemisorption results.

	Pt (wt %)[a]	Pt size by TEM (nm)[b]	Chemisorbed CO (mmol)[c]
PCC-1	0.040	1.18	0.0003
PCC-2	0.164	2.11	0.0013
PCC-3	0.417	3.07	0.0027
PCO-1	0.042	1.13	0.0003
PCO-2	0.179	2.17	0.0014
PCO-3	0.395	3.11	0.0029

[a] The amount of Pt determined by ICP-OES measurement.

[b] An average Pt particle size measured by TEM images.

[c] For estimation of the CO molecules used, 5% CO/He (30 sccm) was injected in a single pulse for 10 s.

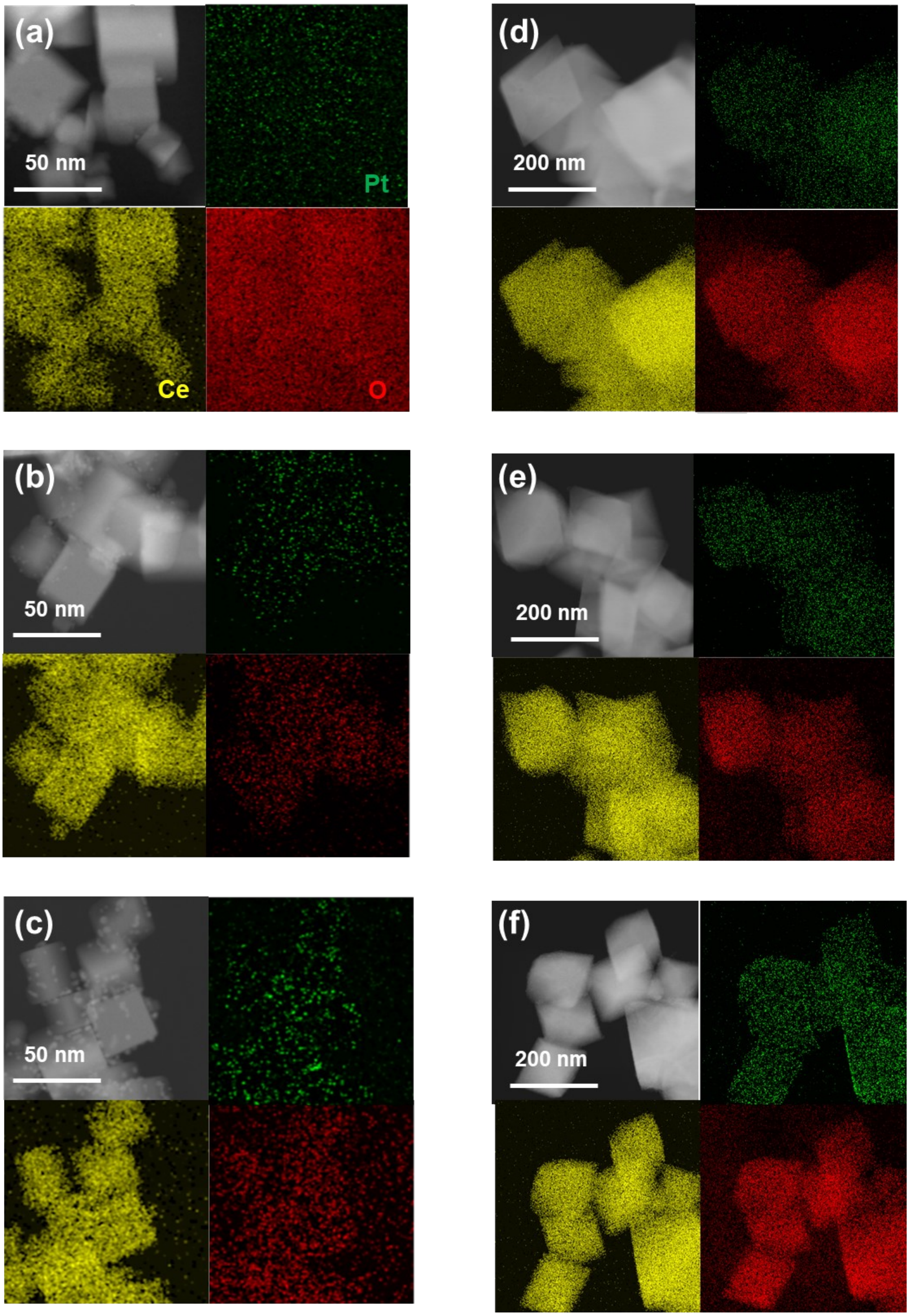

Fig. S3 EDS mapping of Pt/CeO_2 catalysts: (a) PCC-1, (b) PCC-2, (c) PCC-3, (d) PCO-1, (e) PCO-2, and (f) PCO-3.

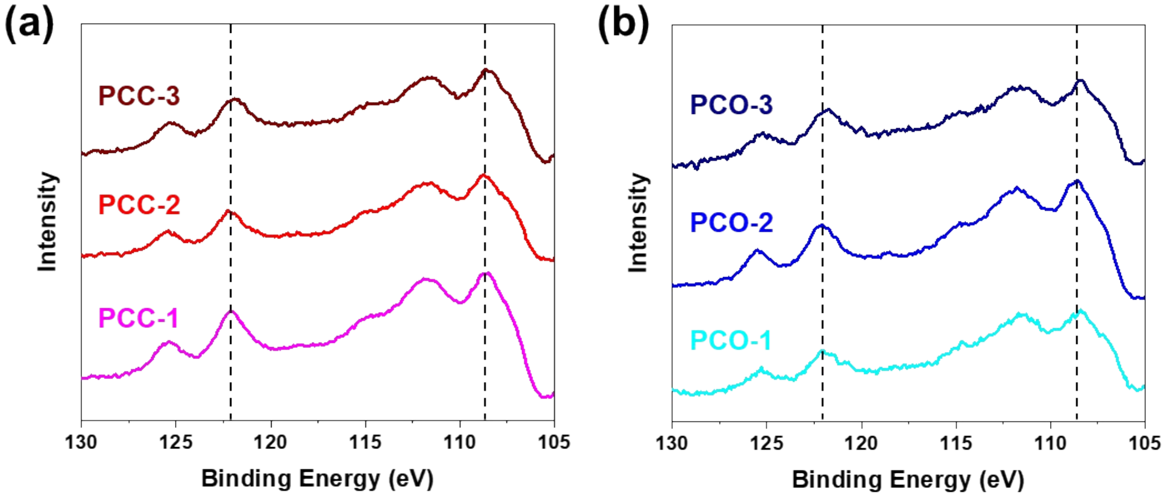

Fig. S4 XPS results for the Ce 4*d* region: (a) Pt/CeO_2-cube, and (b) Pt/CeO_2-octa. The peak position of the Ce 4*d* spectrum is consistent with the Ce^{4+} component at ~ 122 eV.

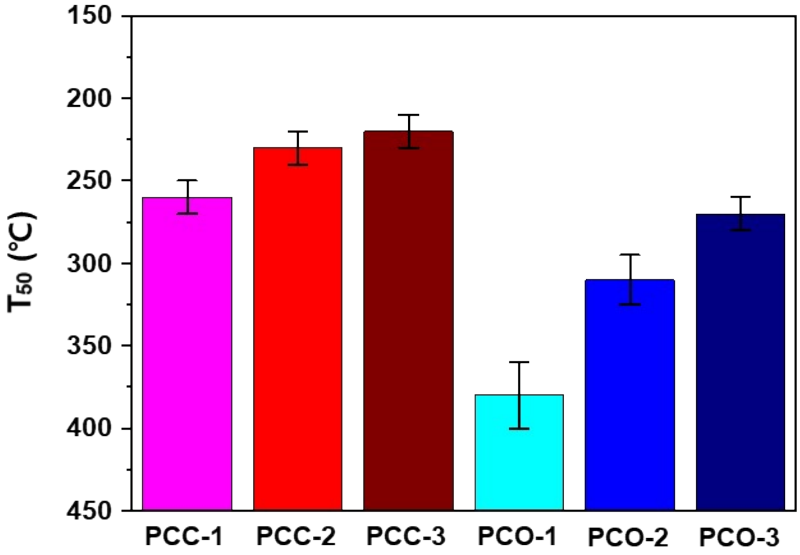

Fig. S5 T_{50}, the temperature at which CO conversion of Pt/CeO_2 catalysts reached 50%.

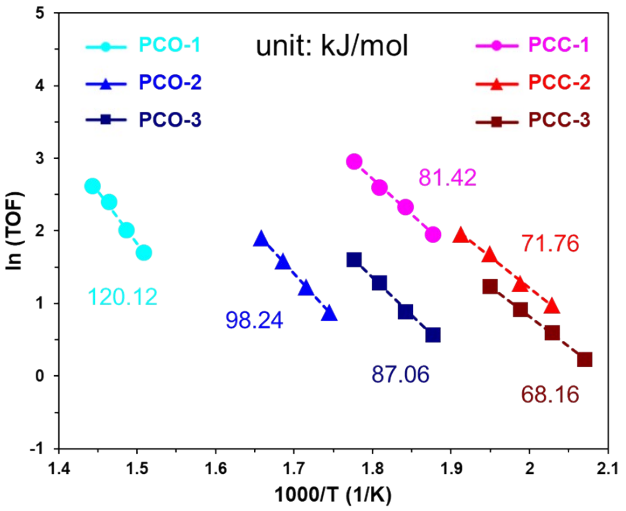

Fig. S6 Arrhenius plot with calculated activation energies. The activation energy was estimated based on the turnover frequency (TOF) from the reaction rate per active site (determined by CO chemisorption) per time. The activation energy gap between PCC and PCO gradually decreases by increasing the size of Pt NPs.

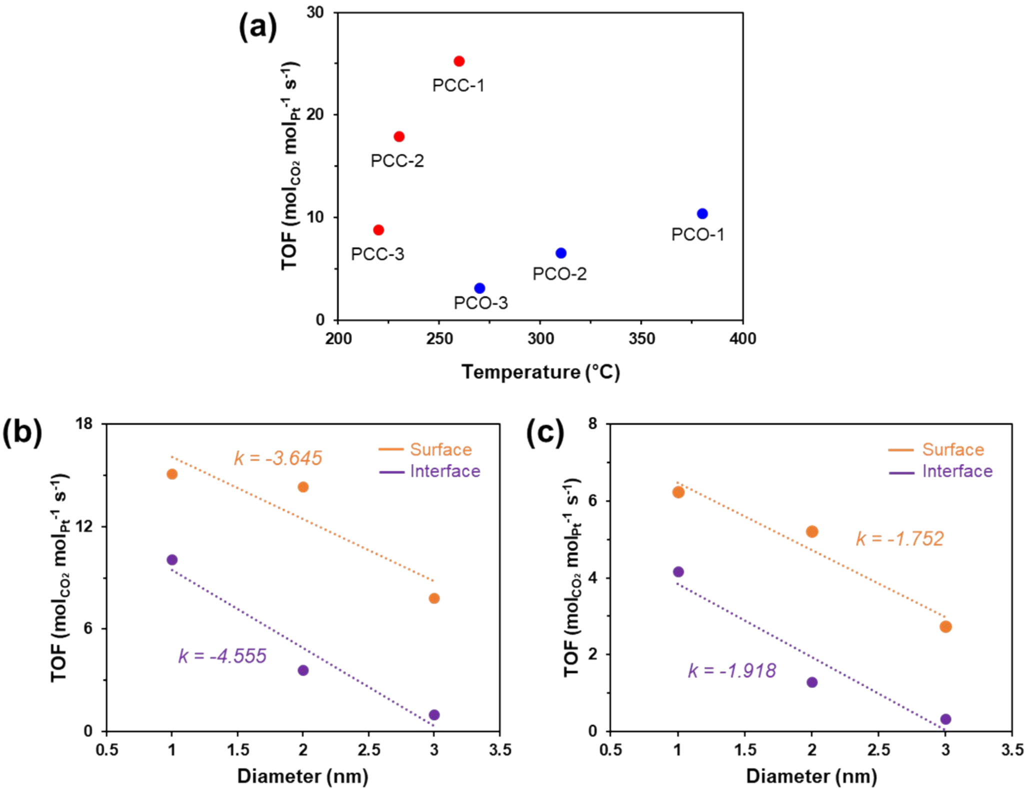

Fig. S7 (a) TOF of Pt/CeO_2 catalysts at 50 % of CO conversion for each catalyst. The site-normalized TOF of surface Pt and interface Pt by the Pt particle size and the corresponding slope in (b) PCC series and (c) PCO series. The proportion of Pt atoms located at the interface was assumed to be 40% at 1 nm, 20% at 2 nm, and 10% at 3 nm.

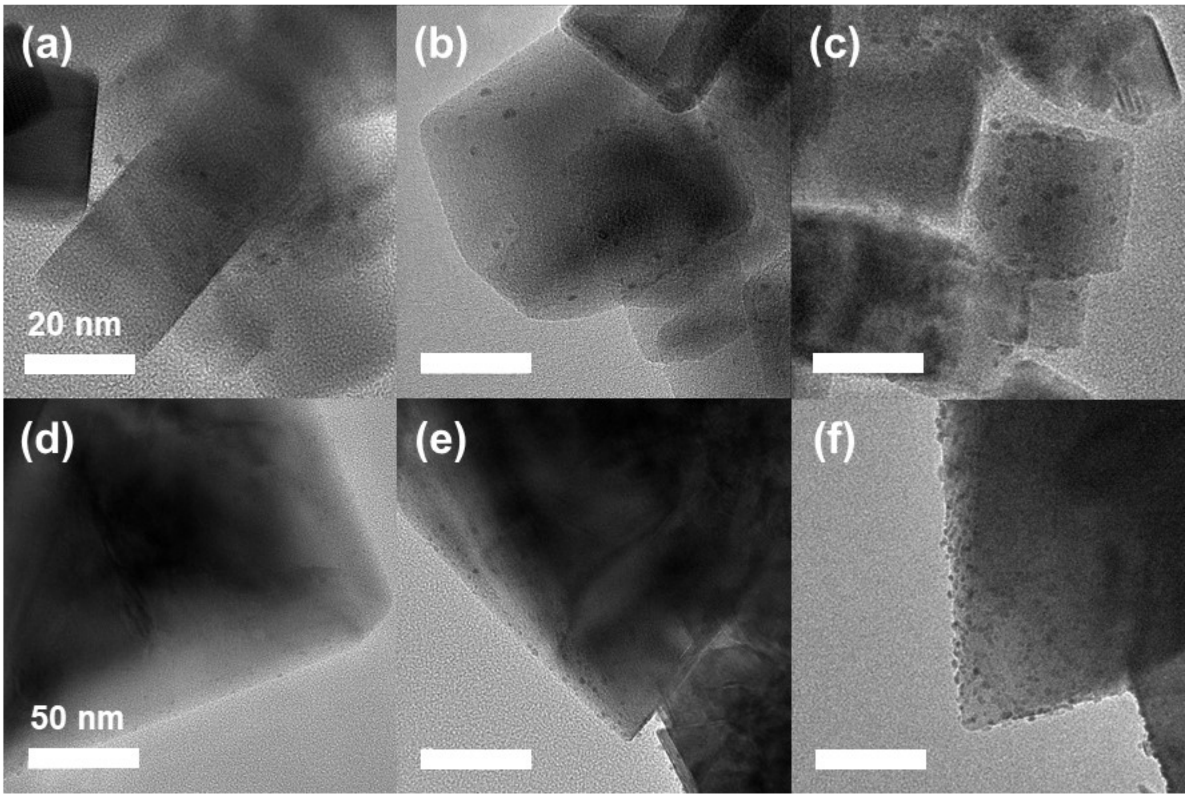

Fig. S8 TEM images of the spent catalysts after reaction: (a) PCC-1, (b) PCC-2, (c) PCC-3, (d) PCO-1, (e) PCO-2, and (f) PCO-3. Scale bars are 20 nm for PCC, and 50 nm for PCO.

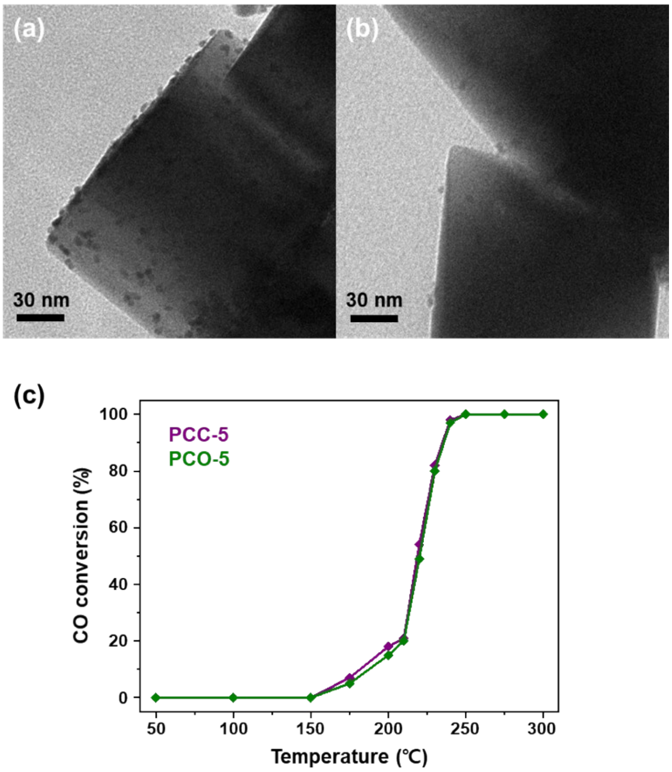

Fig. S9 TEM images of 1% Pt (5 nm) on (a) CeO_2 cubes and (b) CeO_2 octahedra. (c) CO oxidation rates of Pt/CeO_2 catalysts with Pt size of 5 nm.

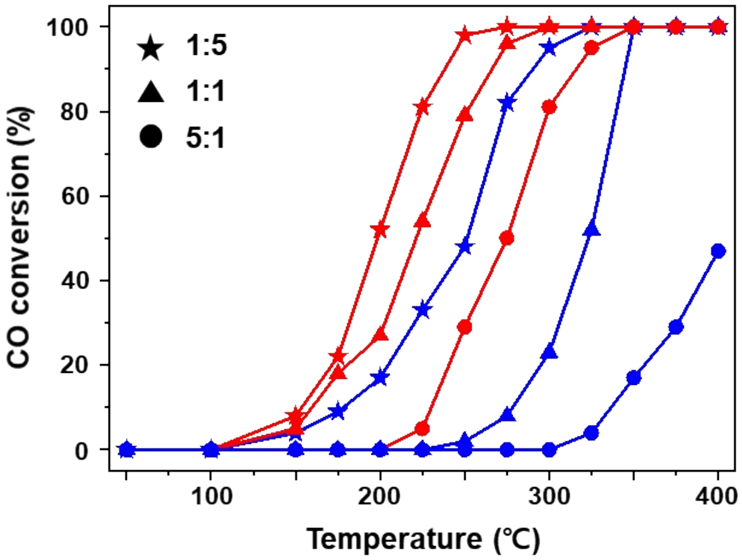

Fig. S10 CO oxidation activity of PCC-2 (red) and PCO-2 (blue) under different ratios of CO and O_2. The CO to O_2 ratio was controlled with 2% CO and 10% O_2 (1:5, star), 2% CO and 2%

O_2 (1:1, triangle), and 10% CO and 2% O_2 (5:1, circle). The reaction gas mixture was balanced with Ar and the total flow was maintained at 50 mL·min^{-1}.

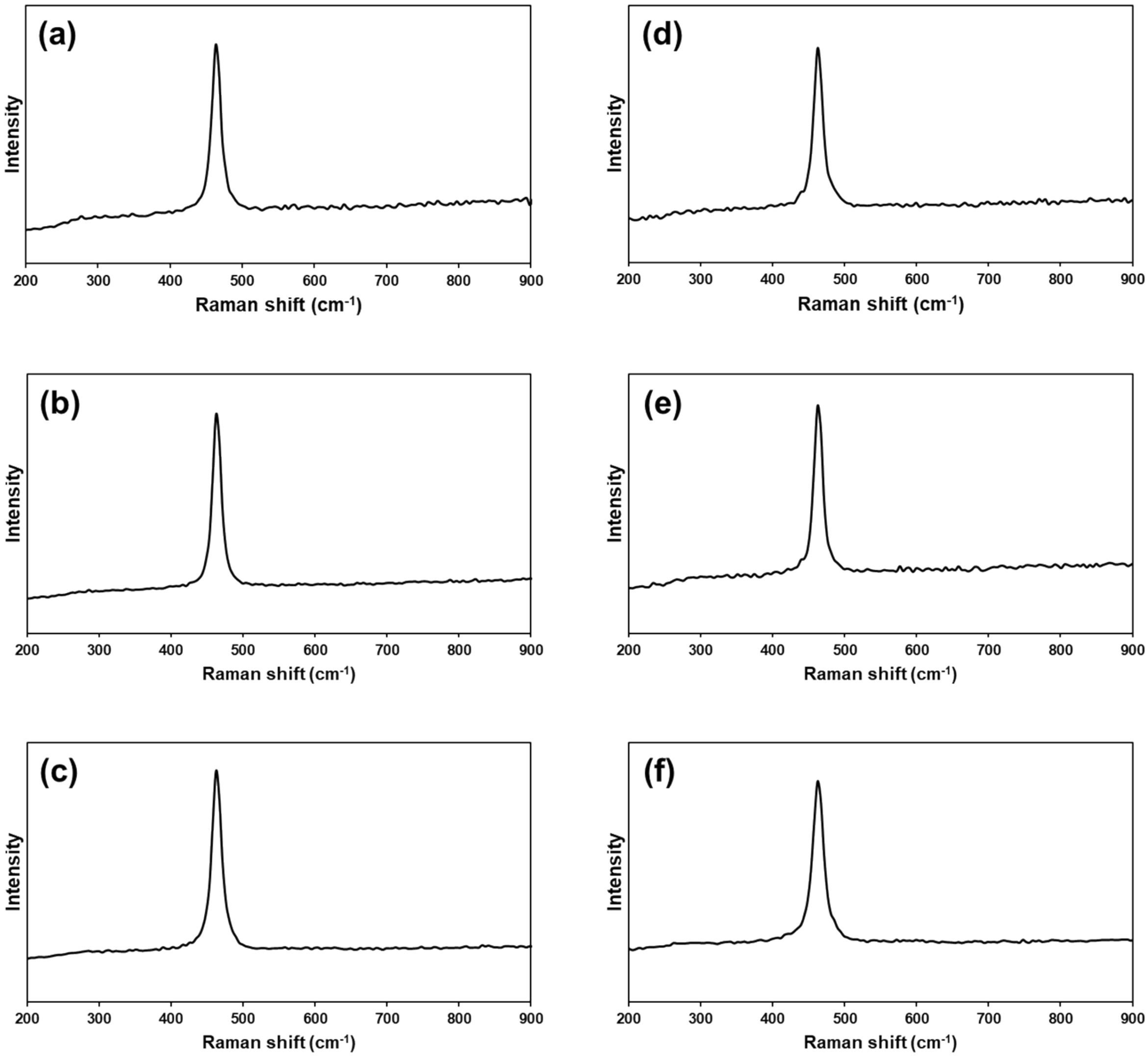

Fig. S11 Raman spectra of Pt/CeO_2 catalysts: (a) PCC-1, (b) PCC-2, (c) PCC-3, (d) PCO-1, (e) PCO-2, and (f) PCO-3.

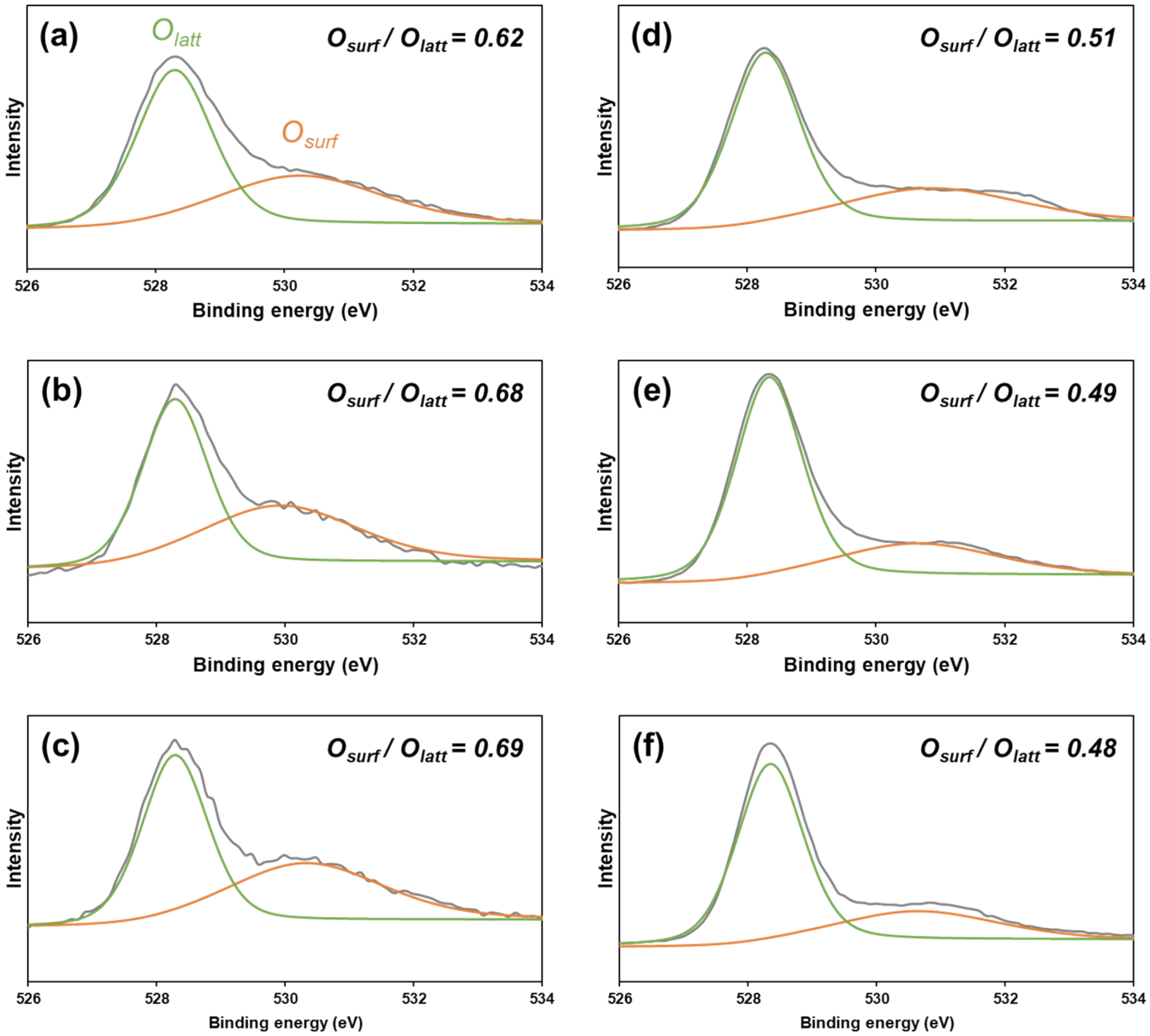

Fig. S12 XPS spectra (O 1*s*) of Pt/CeO_2 catalysts: (a) PCC-1, (b) PCC-2, (c) PCC-3, (d) PCO-1, (e) PCO-2, and (f) PCO-3. Peak deconvolution divided the O 1*s* spectra into the surface oxygen (O_{surf}, orange) and the lattice oxygen (O_{latt}, green).

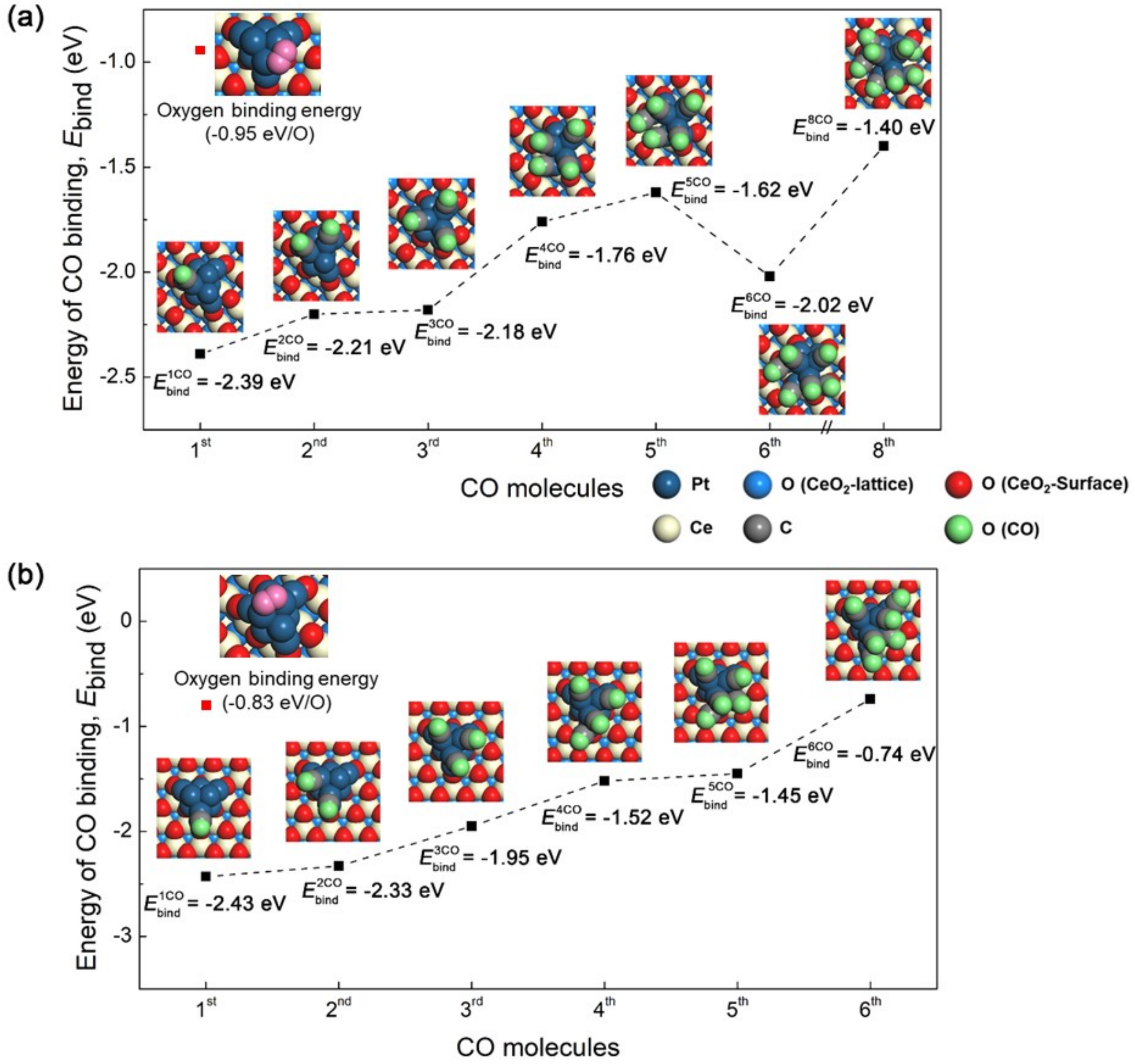

Fig. S13 DFT-calculated energies of sequential CO adsorption over (a) Pt_9-NP/CeO_2(100) and (b) Pt_9-NP/CeO_2(111). The black square E_{bind}^{nCO} denotes the binding energy of the n^{th} CO molecule. The red square represents the O_2 binding energy competing with the first binding CO molecules.

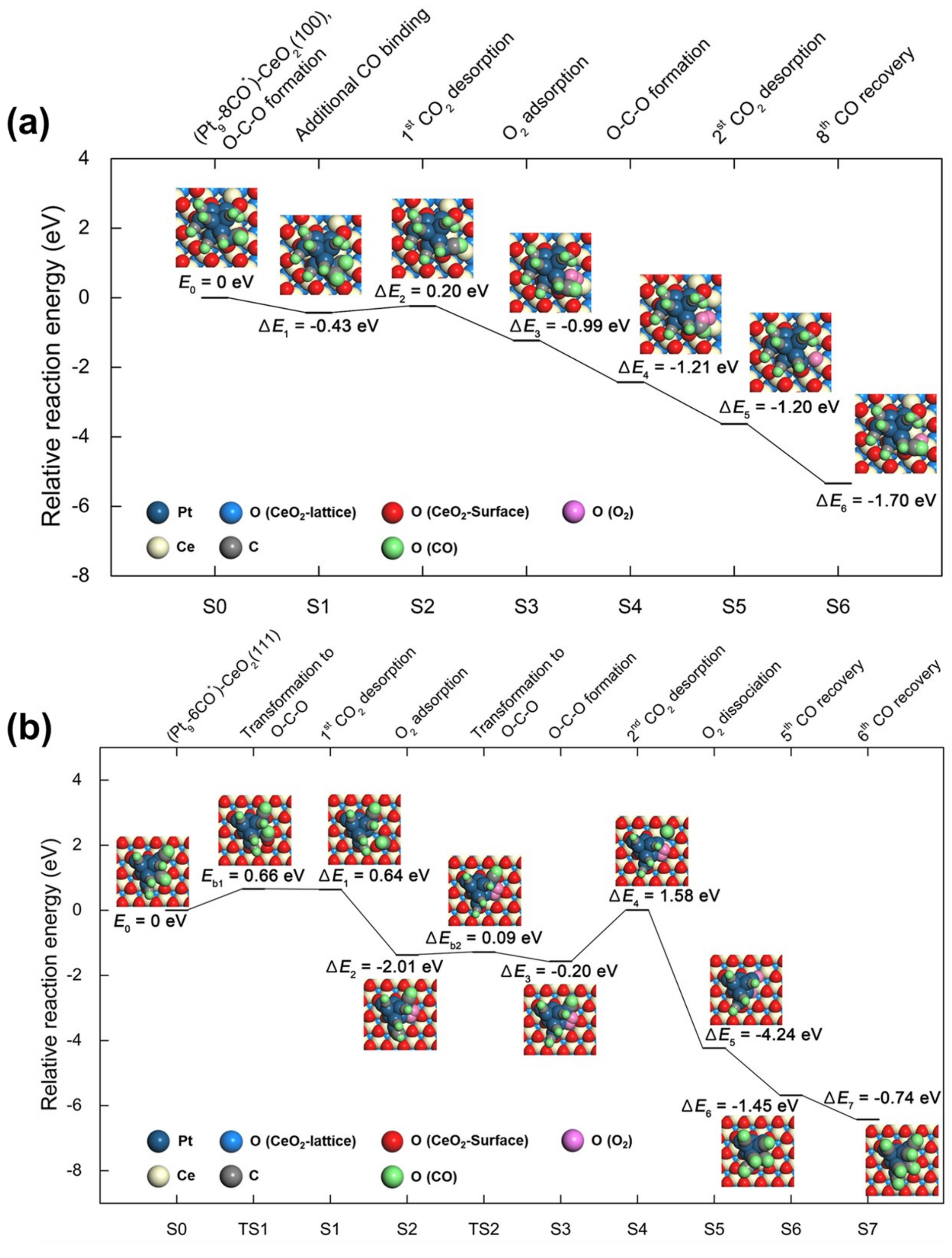

Fig. S14 DFT-estimated CO oxidation pathways for (a) Pt_9-NP/CeO_2(100) and (b) Pt_9-NP /CeO_2(111). The Pt_9-NP/CeO_2(100) interface, which spontaneously forms an O-C-O-type intermediate in the sequential adsorption step of CO molecules, produces CO_2 without a high activation energy barrier. On the other hand, the CO oxidation pathway catalyzed by the Pt_9-NP/CeO_2(111) not only has an activation energy barrier of 0.66 eV, TS1, for O-C-O-type intermediate formation, but also requires a high energy of 1.58 eV, S4, for the 2nd CO_2 desorption.

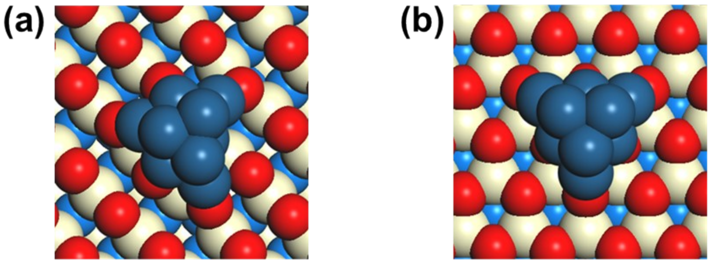

Pt_9-NP/CeO_2(100)
E_{bind} = -8.49 eV

Pt_9-NP/CeO_2(111)
E_{bind} = -8.22 eV

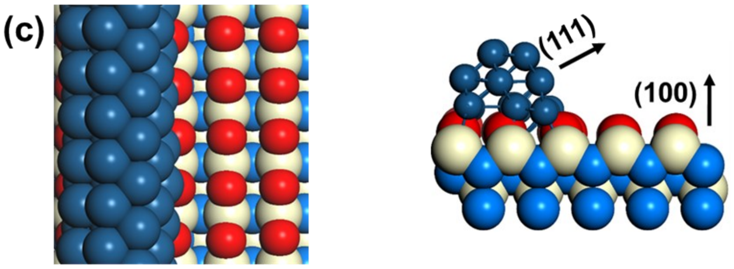

Pt_{56}-rod/CeO_2(100)
E_{bind} = -19.94 eV

Pt_{56}-rod/CeO_2(100)

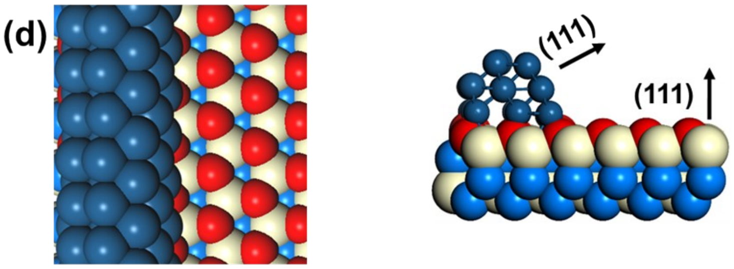

Pt_{56}-rod/CeO_2(111)
E_{bind} = -16.75 eV

Pt_{56}-rod/CeO_2(111)

● Ce ● Pt ● O (surface) ● O (lattice)

Fig. S15 Optimized morphologies and binding energies of Pt_9 NP and Pt_{56} rod supported on CeO_2: (a) Pt_9-NP/CeO_2(100), (b) Pt_9-NP/CeO_2(111), side and top views of (c) Pt_{56}-rod/CeO_2(100) and (d) Pt_{56}-rod/CeO_2(111). Pt_9-NP/CeO_2(100) and Pt_9-NP/CeO_2(111) models are constructed with a two-layered FCC-type Pt_9 NP supported on CeO_2(100) $3 \times 3 \times 2$ slab and CeO_2(111) $5 \times 5 \times 2$ slab. In Pt_{56}-rod/CeO_2 models, a Pt rod containing 56 Pt atoms is supported on CeO_2(100) $5 \times 6 \times 2$ slab and CeO_2(111) $6 \times 6 \times 2$ slab. E_{bind} represents the binding energy of Pt_9 NP and Pt_{56} rod on CeO_2(100) and CeO_2(111), respectively.